Early Views of the Martian Surface from the Mars Orbiter Camera of Mars Global Surveyor

M. C. Malin,* M. H. Carr, G. E. Danielson, M. E. Davies, W. K. Hartmann, A. P. Ingersoll, P. B. James, H. Masursky, A. S. McEwen, L. A. Soderblom, P. Thomas, J. Veverka, M. A. Caplinger, M. A. Ravine, T. A. Soulanille, J. L. Warren

High-resolution images of the martian surface at scales of a few meters show ubiquitous erosional and depositional eolian landforms. Dunes, sandsheets, and drifts are prevalent and exhibit a range of morphology, composition (inferred from albedo), and age (as seen in occurrences of different dune orientations at the same location). Steep walls of topographic depressions such as canyons, valleys, and impact craters show the martian crust to be stratified at scales of a few tens of meters. The south polar layered terrain and superposed permanent ice cap display diverse surface textures that may reflect the complex interplay of volatile and non-volatile components. Low resolution regional views of the planet provide synoptic observations of polar cap retreat, condensate clouds, and the lifecycle of local and regional dust storms.

The Mars Orbiter Camera (MOC) aboard the Mars Global Surveyor (MGS) spacecraft provides imaging observations at two scales. The narrow-angle (NA) high-resolution camera (3.7 μradians per pixel) provides views down to 1.5 m per pixel of small areas. These views are usually acquired as long, narrow north-south strips several kilometers wide and several tens of kilometers long. The two wide angle cameras (WA) use 140° field-of-view (FOV) lenses to view the planet, in red and blue wavelengths (bandpasses ~0.60 to 0.63 μm and ~0.42 to 0.45 μm), from horizon to horizon (down to 230 m/pixel at nadir and 1.5 km/pixel at the limb). MOC images are acquired one line at a time as the spacecraft motion sweeps the FOVs across Mars (*1*).

Images discussed here were collected between 15 September 1997 and 15 January 1998, during the first 100 MGS orbits, shortly after each periapsis, as the MOC FOV was slewed perpendicular to the orientation of the line-array detectors. When aerobraking was temporarily halted between orbits 19 through 35, nadir-oriented images were built-up with spacecraft orbital motion rather than by slewing. Depending on the start time, duration, and rate of slew, the highest-resolution NA images are 3 to 4 m/pixel with emission angles of 0° to 90°. Owing to the non-standard conditions (altitude/velocity) of the aerobraking orbits compared to the final mapping orbit, the original pixels have aspect ratios of typically ~1.5:1 but exceed 5:1 in some cases; the images shown have been resampled to yield equant pixels and the lower, final, effective resolution is reported in meters per pixel along with frame width versus height in kilometers. During the final MGS mapping orbit, MOC images of about three times higher resolution will be required.

Eolian landforms. Wind is an effective geologic agent on Mars because of the long time scales for landform development. This is facilitated by the lack of plate tectonics and by the low rates or lack of competing fluvial and volcanic processes in the latter half of Mars's history (*2*). Long-term variations in the effectiveness of the wind may also be driven by changes in atmospheric pressure that affect the temperatures, dust loading, and thermal response times of the atmosphere (*3*). Periodic variations in climate are imposed by orbital cycles, which determine the season at which perihelion occurs, and currently produce a significant north-south asymmetry in climate and wind directions with a 51,000-year period (*4*).

The MOC images confirm suggestions from earlier spacecraft observations that much of Mars is pervaded by erosional and depositional eolian landforms. The Medusae Fossae Formation (MFF), a major unit of relatively young, indurated but easily erodible materials that occur near the equator (*5*, *6*), dominates an area on the

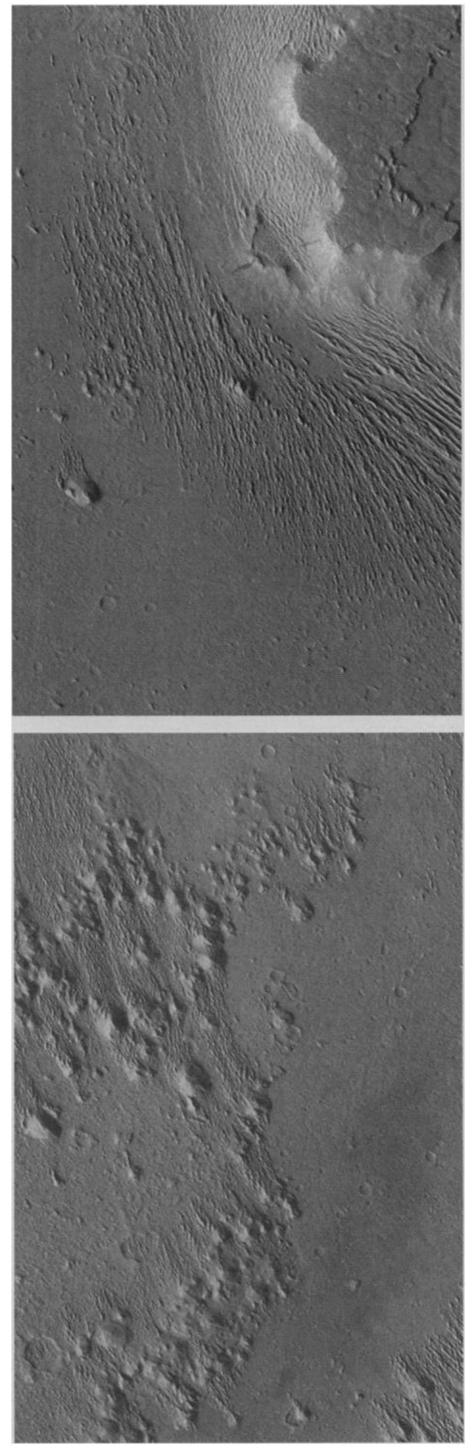

Fig. 1. Extensive windswept plains of the Medusae Fossae Formation. (**A**) Northern subframe (frame 3104; ~5 m/pixel; 3.0 x 4.7 km area centered near 2.4°N, 163.8°W); (**B**) southern subframe (frame 3104; ~5 m/pixel; 3.0 x 4.7 km area centered near 2.0°N, 163.8°).

M. C. Malin, M. A Caplinger, M. A. Ravine, J. L. Warren, Malin Space Science Systems, Post Office Box 910148, San Diego, CA 92191–0148, USA.
M. H. Carr, U.S. Geological Survey, Menlo Park, CA 94025, USA.
G. E. Danielson and A. P. Ingersoll, Division of Geological and Planetary Sciences, California Institute of Technology, Pasadena, CA 91125, USA.
M. E. Davies, The Rand Corporation, Santa Monica, CA 90406–2138, USA.
W. K. Hartmann, Planetary Science Institute, Tucson, AZ 85719, USA.
P. B. James, Department of Physics and Astronomy, University of Toledo, Toledo, OH 43606, USA.
H. Masursky (deceased) and L. A. Soderblom, U.S. Geological Survey, Flagstaff, AZ 86001, USA.
A. S. McEwen, Lunar and Planetary Laboratory, University of Arizona, Tucson, AZ 85721–0092, USA.
P. Thomas and J. Veverka, Center for Radiophysics and Space Research, Cornell University, Ithaca, NY 14853, USA.
T. A. Soulanille, Prama Corporation, Pasadena, CA 91116–6077, USA.
*To whom correspondence should be addressed.

southern edge of the Amazonis basin (Fig. 1). These deposits show evidence of wind erosion that formed curvilinear ridges and grooves on the surface. They have such low radar reflectivities (*7*) that they have been nicknamed the "Stealth" deposits. Peripheral to the main unit are pedestal craters, mounds within craters, low ridges forming rectilinear patterns, sinuous ridges, and discontinuous remnants of the deposits; the subjacent terrain is visible in local hollows. These characteristics have all been interpreted as indicative of MFF remnants on a wind-stripped or exhumed surface (*6, 8, 9*).

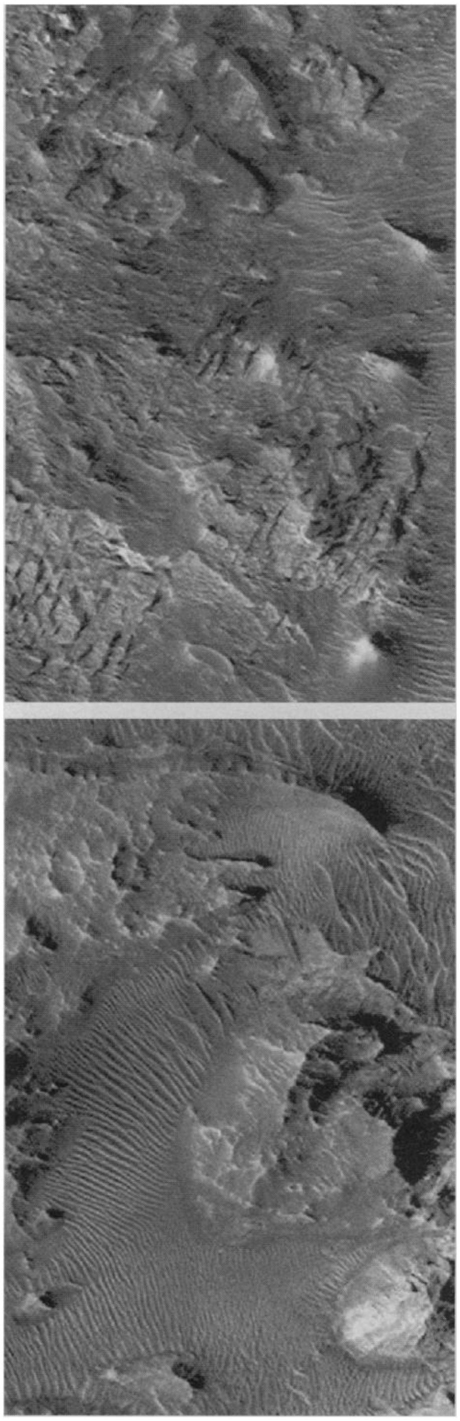

Fig. 2. Complex variations in dune forms within Hebes Chasma. (**A**) Northern subframe (frame 3506; ~5 m/pixel; 2.3 x 3.6 km area centered near 0.6°S, 76.3°W); (**B**) southern subframe (frame 3506; ~5 m/pixel; 2.3 x 3.6 km area centered near 0.8°S, 76.3°W).

Impact craters on the remnant mesas of the MFF (Fig. 1A) indicate that the deposits were stable for a significant length of time before the erosion began. This cratered upper surface forms a cap rock that, when breached, exposes deeper, less indurated material. The easily erodible deposits have been carved into intricate patterns by the wind; where most of the deposit has been removed, the underlying cratered plains are exposed. In some areas the MFF appears to be layered. The MFF has variously been interpreted as volcanic ash deposits (*10*), an analog to the polar layered deposits but present now at the equator as a result of polar wander (*9*), and simply as thick deposits of eroded and weathered debris that formed early in the history of the planet, when erosion rates were high, and that have been moved around the planet ever since, as global wind patterns changed (*8, 11*).

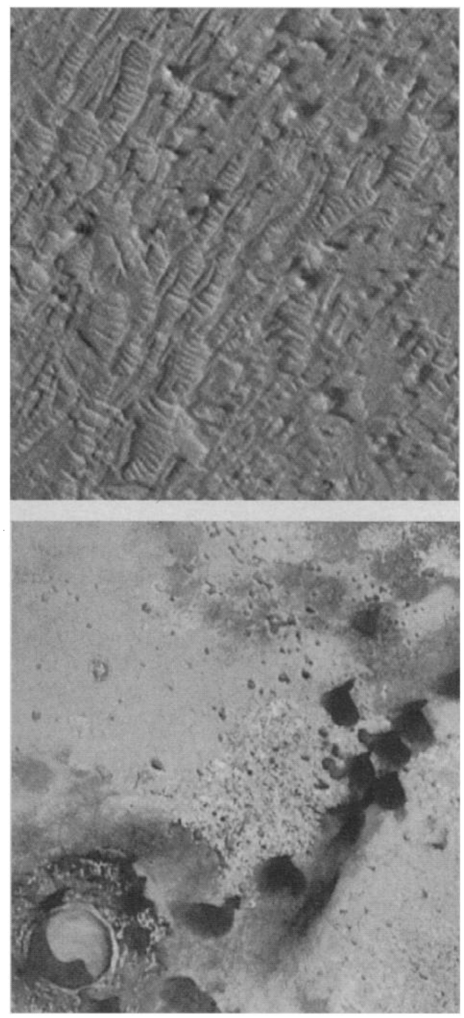

Fig. 3. (**A**) Dunes in etch pits and troughs in Crommelin crater in the Oxia Palus area (frame 3001; ~5 m/pixel; 3.2 x 3.5 km area centered near 4.1°N, 5.3°W); (**B**) Rare tear-shaped dark dunes (frame 10004; ~10 m/pixel; 6.4 x 7.0 km area centered near 47° S, 341° W).

The MOC NA images show that most of the regions observed at the scale of meters are dominated by eolian deposits—dunes (of a wide variety of forms), drifts, and debris mantles devoid of bedforms (to the limit of resolution)—varying in scale, morphology, age, and albedo (Figs. 1 to 3). Sediment thicknesses of meters or more (as estimated from topographic in-filling) are common. Dunes and drifts are usually abundant at the meter scale even in those regions that are predominantly undergoing wind erosion (Fig. 3A). Such MOC images show the dramatic effectiveness of topography in trapping eolian materials. Many areas show a composite of dunes that are undergoing erosion (ragged shapes, rounded crests, and so forth) and others whose forms (for example, crescentic shape, strongly demarked stoss and lee slopes, and so forth) suggest that they are currently active.

Complex forms seen in MOC images indicate that some eolian features were formed in wind regimes different from the present. Most dunes on Mars are transverse, consistent with unidirectional winds indicated by wind streaks and predicted by general circulation models of the current climate (*12*). However, in many places the MOC images show juxtaposition of fresh and degraded dune forms, including probable star dunes and multiple transverse dune sets, indicating episodes of multiple wind direction and providing expanded evidence for dunes formed by complex winds (*12–14*). These complex wind systems could arise from periodic changes in the season at which perihelion occurs (51,000-year cycle) or from secular changes in the orbit and inclination, or atmospheric pressure.

In many areas bright and dark dunes exist; commonly, their patterns are superposed and crossing (Fig. 2A). The wide range of albedos suggests that they vary widely in their composition and physical makeup. Most large dune fields recognized in Viking images are relatively dark and have been hypothesized to contain mafic materials, possibly basalt (*15*). Some studies of high-resolution Viking data had suggested that bright dunes are dark dunes covered by bright dust (*16*). However, many of the bright dunes seen in MOC NA images are brighter than the interdune areas; this contrast indicates that the higher albedo cannot be attributed to a blanket of bright dust. In many places both bright and dark transverse dunes superpose on one another, indicating local diversity of dune age and composition. These findings indicate the availability of a wide range of materials that form saltating particles on Mars.

Layering in the upper crust of Mars. MOC NA images acquired at 5 to 10 m/pixel resolution (and extending from about 40° to 90°W longitude) show that layering is ubiquitous within the walls of Valles Marineris. Layering is seen, where bedrock is exposed throughout the entire depth of the canyon, in places several kilometers below the plateau surface (Fig. 4A). The dominant morphology of the chasma walls consists of steep spurs and gullies (*17*); at all locations imaged at better than 10 m/pixel by MOC, the spurs consist of layers varying from a few meters to 50 m in thickness.

Viking and Mariner images delineated only an uppermost zone of the crust about 0.5 km thick, and dark layers were seen in the south Coprates Chasma and the north wall of Ophir Chasma (*18*). Previous investigations inferred that this stratigraphy reflected ~0.5-km-thick layered lavas overlying predominantly impact megabreccias generated during the late heavy bombardment–megabreccias that, although never directly observed, are believed to be only crudely layered (*17*, *19*, *20*). In contrast, MOC NA images show that where exposed, the wall rock exhibits well-defined layering on a few to a few tens of meters scale. We assume that the layers, particularly those at depths of several kilometers below the plateau surface, belong to the ancient Upper Noachian or Lower Hesperian stratigraphic series (thought to be 3.5 to 4.3 billion years old), because they underlie the Lower Hesperian ridged plains material (*20*) but do not appear to be modified by late heavy bombardment.

The composition of the layers is unknown. They consist of alternate dark ledges and brighter slopes. The brighter slopes generally appear to be colluvial debris mantled by eolian dust. However, in some places, there appear to be brighter layers of in situ bedrock, implying variation in the composition of the layers. One hypothesis for these layers is that they are predominantly volcanic flows, perhaps with intercalated horizons of regolith, pyroclastic volcanic rocks, or sedimentary rocks. Arguments favoring this view include: (i) the overlying geologic units over most of the area are volcanic flows (*21*), (ii) there is evidence that the walls are rich in pyroxene, a common igneous mineral (*22*), (iii) the layer thicknesses and ledge-forming topography are similar to those seen in some terrestrial flood basalts like those of the Columbia River basalts (*23*), and (iv) high heat flows on Mars during this time period might be expected to produce such voluminous volcanism (*24*).

Another hypothesis is that the layers represent the accumulation of wind or water-lain deposits, or both, formed perhaps within a basin or regional depression at one time occupied by a standing body of water. Arguments favoring these ideas include: (i) the similarity in the appearance of the layers to that of many terrestrial sedimentary deposits and (ii) the apparent lateral extent of the layering. It seems unlikely that a several-kilometers-thick section of sedimentary rocks could have accumulated during this period of martian geologic history without evidence of these laterally extensive deposits elsewhere in Mars's geological record.

Layered units within the interior of some of the chasmata were observed in Mariner 9 images (*25*). Subsequent Viking observations delineated their spatial distribution (for example, *26*) and provided evidence of alternating bands of units with different albedos, layers of varied thickness, yardangs, and mass-wasted gullies (*17*). These deposits post-date the formation of the canyons. MOC images of a section of chasm-fill within Candor Chasma (Fig. 4B) suggest that the layered materials differentially eroded at small scales. The exact relationships are often obscured by eolian mantles or dunes, whose materials may or may not be derived from the underlying units.

Polar terrains. The martian polar regions have been a target of scientific focus for centuries, dating back to early telescopic observations that revealed the Earth-like seasonal progression in the formation and disappearance of polar hoods and ice caps. Early spacecraft reconnaissance showed the terrains on which the seasonal and permanent polar ice rested to consist at each pole of a complex of layered deposits (*27*), each 1000 to 2000 km in lateral extent and perhaps several kilometers thick (*28*). Layers in the polar deposits consist of horizontal units, typically tens of meters in thickness, that outcrop as light and dark bands, often with alternating cliff-and-terrace relief, along sinuous outer margins and valleys cutting down into the deposits (*29*). The low crater populations of the layered terrains suggest that they are young on the martian geologic time scale (*30*). Seasonal frost (largely CO_2, with traces of water) forms each winter and reaches latitudes down to ~60°. This deposit then sublimes each spring, leaving a permanent, residual ice cap. The summer equilibrium temperature of the north polar permanent cap suggests that it is composed of water ice, while the temperature for the south polar cap implies CO_2 ice (the CO_2 ice at least surficially mantles the cap, although water-ice may be present below this mantle) (*31*). In some places polar layered terrains rest, often unconformably, on older units that exhibit

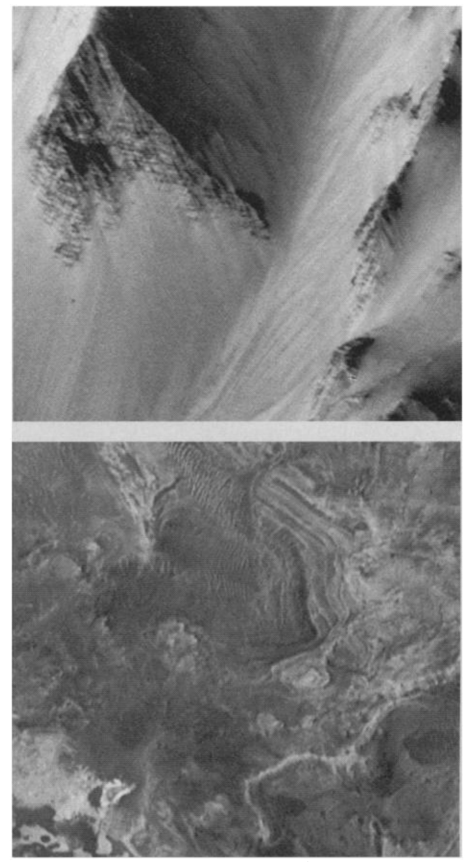

Fig. 4. (**A**) Banded outcrops in walls of Tithonium Chasma/Ius Chasma section of Valles Marineris (frame 1303; ~10 m/pixel; 4.6 x 4.3 km area centered near 6.6°S, 90.4°W); (**B**) complex central deposits in floor of Candor Chasma section of Valles Marineris (frame 8405; ~7 m/pixel; 3.3 x 3.1 km area centered near 6.7°S, 75.4°W).

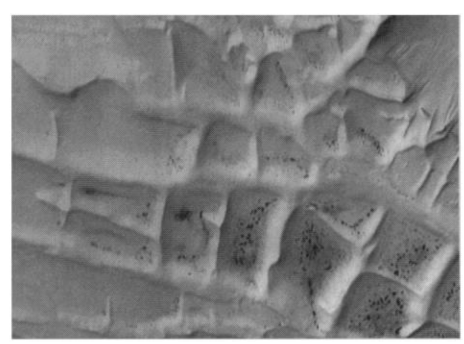

Fig. 5. Complex of rectilinear intersecting ridges in the south polar region (frame 7908; ~23 m/pixel; 20 x 14 km area centered near 81.5°S, 65°W).

varying degrees of preservation (*32*). These older units include ancient cratered terrains in the south and cratered plains in the north. The layered deposits are speculated to contain detailed climatologic records for Mars's recent geologic past; those in the south are thought to be of order 100 million years old (*33*).

MOC NA images of the southern polar terrains (Figs. 5 and 6) were obtained during late southern spring (L_s ~245°) as the seasonal CO_2 ice deposits were in the early stage of subliming and at a time after the south polar hood had dissipated and the atmosphere was fairly clear. All the areas shown were still coated with the annual CO_2 frost deposit. A complex of ridges that intersect in a rectilinear pattern (Fig. 5) may be remnants of an old deposit that rests stratigraphically below the southern polar layered deposit. Such old mantling deposits may represent reworked material from even more ancient polar layered complexes. The origin of the ridges is unclear—they may be eolian mantles lithified by cementation or ice accumulation, with the intervening materials deflated by wind action. Some of their characteristics resemble dunes, and there may be more than one process at work in their formation. The dark spots within the ridge area are enigmatic; they are 20 to 100 m across. Because this region was still covered by seasonal CO_2 frost, these discrete features evidently defrost early.

Some surfaces within the area of the south polar layered terrain associated with the permanent ice cap (Fig. 6) show rugged scalloped textures, whereas others are smooth and nearly featureless. This suggests that the strength and character of the layers within the deposits are variable. This variation is also evident on the terraces and benches, where layers of different resistance outcrop along the sinuous slopes within the deposit. The textures seen on surfaces between layered slopes are scalloped, mottled lower surfaces and superposed smooth-surfaced small mesas rimmed by arcuate cliffs (Fig. 6) in areas within the permanent cap. These resemble some sublimation and ablation features seen in terrestrial glacial ice and may reflect the thickness of water or CO_2 ice above the underlying layered deposits.

South polar cap recession. MOC imaged the annual recession of the CO_2 south polar cap during early southern spring. This is the first recession observed by spacecraft since the 1977 Viking observations (*34*). These data allow examination of interan-

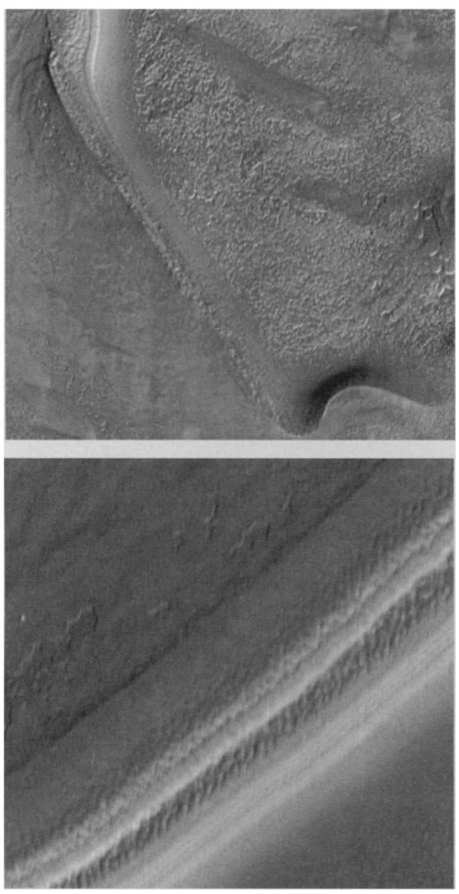

Fig. 6. Textures of the south polar permanent residual ice cap and polar layered terrains. (**A**) Frame 7709; ~51 m/pixel; 30 x 29 km area centered near 87°S, 77°W; (**B**) Frame 7306; ~25 m/pixel; 15 x 14 km area centered near 87°S, 341°W.

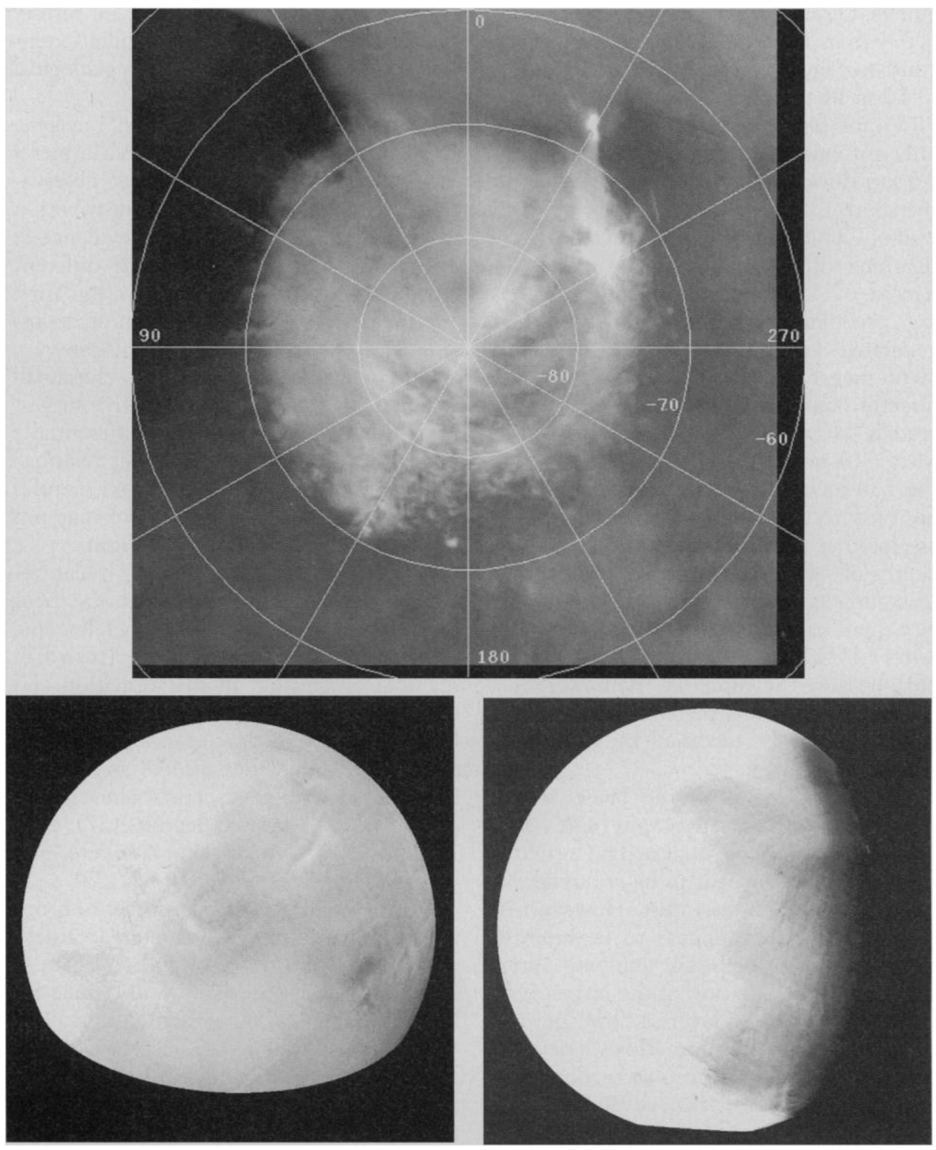

Fig. 7. (**A**) Polar stereographic mosaic of the seasonal south polar region (MOC WA red images from orbits 67 through 73); (**B**) color composite of condensate clouds over Tharsis made from red and blue images with a synthesized green channel (MOC WA frames from orbit 48); (**C**) blue-filter image of the 1997 martian dust storm (MOC WA frame from orbit 50).

nual variations in the retreat (35). Variation in dust storm activity during early southern spring might be expected to affect the seasonal sublimation of the south polar cap by modifying the energy balance at the surface (34). The 1997 dust storm was different from that of 1977. In 1977, a major storm was first observed at $L_s = 205°$ (36) in the Thaumasia region; it expanded rapidly through the southern hemisphere and then into the northern hemisphere, whereupon dust was observed at both Viking landing sites (37). During 1997 the southern hemisphere remained clear until after $L_s = 220°$; subsequently, considerable dust was seen over and around the cap as well as in Noachis. The influence of the timing and intensity of dust storms should be revealed by comparing the MOC and Viking data sets. Two synoptic views of the south polar cap by Viking during this season, at $L_s = 221°$ and 237°, were compared with polar stereographic projections of MOC images of the cap at $L_s = 221°$ and 238-244° (for the mosaic in Fig. 7A). The bright peninsula of frost extending from the cap (~70°S, 320°W) is known historically as the Mountains of Mitchel. The position and detailed character of the edge of the frost cap (that is, its relation to small craters and character of small frost outliers) were found to be similar in the Viking and MGS images. The annual CO_2 sublimation is largely unaffected by major variations in annual dust storm activity. This observation will place important constraints on radiative transfer and atmospheric thermal transport processes (38).

Condensate clouds. The MOC aerobraking imaging period occurred during early southern spring, during which condensate clouds were often seen in images of the Tharsis region. At L_s ~223° clouds covered Tharsis from the southern extent of Arsia Mons northward through the saddle between Pavonis Mons and Ascraeus Mons (Fig. 7B). The clouds were sufficiently thick to obscure the summit of Arsia in the blue WA image. Opacity was maximum in the eastern part of the saddle between Arsia and Pavonis. The clouds over Tharsis showed small-wavelength wave structure with crests perpendicular to the Tharsis ridge. A plume extended to the east of the summit of Pavonis Mons where it merged into a diffuse wave pattern. An unusual Y-shaped rift in the clouds could be due to either local downwelling induced by the Tharsis topographic high or to a thermally induced diurnal katabatic wind, as was interpreted for similar features seen by Viking (39). Faint hazes, visible primarily in images acquired by the blue WA camera, were seen in many other areas. These, too, were presumably condensate clouds, as they disappeared during the dust storm that developed in Noachis in late November 1997, but reappeared several weeks after the storm subsided.

Dust storms. The MOC WA monitored a dust storm on orbits 50-54 (27 November to 2 December 1997). In the past, southern spring has been the period of the onset of maximum dust storm activity (40). This active period includes the time of Mars perihelion passage ($L_s = 251°$) and extends past the solstice ($L_s = 270°$) into the southern summer.

The November 1997 dust storm could be classified as "regional" in scale. At its peak on orbits 50 and 51 (Fig. 7C), it extended from 25° to 60°S and from 15°W to 40°E, a distance of 2500 km. Although the dust spread farther on subsequent orbits, it seemed to fade into a background dustiness that persisted for several weeks afterward. At the altitude of the spacecraft (124 km), the dust storm caused orbit-to-orbit variations in atmospheric density by factors of 2 or more (41).

Shortly before the storm began, MOC observations indicated small dust storms along the margin of the retreating south polar seasonal cap and within a zone about 5° in latitude from the cap edge. Condensate clouds were seen in Tharsis (as noted above) and Elysium, and condensate hazes were observed in many places. Within 4 days of the storm's outbreak, condensate clouds were no longer seen anywhere on the planet—even in locations where the atmosphere showed no visible traces of increased dust content. Shortly afterward, the small local dust storms along the edge of the retreating cap ceased to form. High-altitude (detached) limb hazes were first seen about 10 days after the storm started. After the storm subsided (evidenced by the dissipation of concentrated vertical and horizontal plumes), the atmospheric opacity remained elevated for several weeks. However, within a month, condensate clouds returned to Tharsis and Elysium, followed shortly thereafter by the frost-cap marginal local dust storms.

REFERENCES AND NOTES

1. M. C. Malin, G. E. Danielson, M. A. Ravine, T. A. Soulanille, *Int. J. Imaging Sys. Tech.* **3**, 76 (1991); M. C. Malin *et al.*, *J. Geophys. Res.* **97**, 7699 (1992).
2. R. Greeley, *Science* **236**, 1653 (1987).
3. R. W. Zurek *et al.*, in *Mars*, H. H. Kieffer, B. M. Jakosky, C. W. Snyder, M. S. Matthews, Eds. (Univ. of Arizona Press, Tucson, AZ, 1992), pp. 835–933.
4. H. H. Kieffer and A. P. Zent, in (3), pp. 1180–1218.
5. M. C. Malin, Second International Colloquium on Mars, Pasadena, CA, 15 to 18 January 1979, *NASA Conf. Publ.* **2072**, 54 (1979).
6. K. L. Tanaka, *J. Geophys. Res.* **91**, E139 (1986); D. H. Scott and K. L. Tanaka, *U.S. Geol. Surv. Misc. Map I-1802-A* (1986); R. Greeley and J. E. Guest, *U.S. Geol. Surv. Misc. Inv. Map 1802-B* (1987).
7. D. O. Muhleman, B. J. Butler, A. W. Grossman, M. A. Slade, *Science* **253**, 1508 (1991).
8. M. H. Carr, *The Surface of Mars* (Yale Univ. Press, New Haven, CT, 1981).
9. P. H. Schultz and A. B. Lutz, *Icarus* **73**, 91 (1988).
10. D. H. Scott and K. L Tanaka, *J. Geophys. Res.* **87**, 1179 (1982).
11. M. H. Carr, *Water on Mars* (Oxford Univ. Press, New York, 1996).
12. P. L. Lee and P. C. Thomas, *J. Geophys. Res.* **100**, 5381 (1995).
13. K. S. Edgett and D. G. Blumberg, *Icarus* **112**, 448 (1994).
14. R. Greeley, A. Skypeck, J. B. Pollack, *J. Geophys. Res.* **98**, 3183 (1993).
15. J. F. Bell III *et al.*, *Lunar Planet. Sci.* **28**, 87 (1997).
16. A. W. Ward *et al.*, *J. Geophys. Res.* **90**, 2038 (1985); J. R. Zimbelman, *Icarus* **71**, 257 (1987); K. S. Edgett, *ibid.*, in press.
17. B. K. Lucchitta *et al.*, in (3), pp. 453–492.
18. P. E. Geissler, R. B. Singer, B. K. Lucchitta, *J. Geophys. Res.* **95**, 14399 (1990).
19. K. L. Tanaka, D. H. Scott, R. Greeley, in (3), pp. 345–382; S. W. Squyres, S. M. Clifford, R. O. Kuzmin, J. R. Zimbelman, F. M. Costard, in (3), pp. 523–556.
20. K. L. Tanaka and M. P. Golombek, *Proc. Lunar Planet. Sci. Conf.* **19**, 383 (1989).
21. D. H. Scott and K. L. Tanaka, *U.S. Geol. Surv. Misc. Inv. Series Map I-1802-A* (1986).
22. S. Erard *et al.*, *Proc. Lunar Planet. Sci. Conf.* **21**, 437 (1991).
23. V. R. Baker and D. Nummedal, *The Channeled Scabland* (NASA, Washington, DC, 1978); J. J. Mahoney and N. F. Coffin, Eds., *Geophys. Monogr. Ser.* 100 (1997).
24. G. Schubert, S. C. Solomon, D. L. Turcotte, M. J. Drake, N. H. Sleep, in (3), pp. 147–183.
25. J. F. McCauley *et al.*, *Icarus* **17**, 289 (1972); R. P. Sharp, *J. Geophys. Res.* **78**, 4063 (1973).
26. S. S. Nedell, S. W. Squyres, D. W. Andersen, *Icarus* **70**, 409 (1987).
27. P. Thomas, S. Squyres, K. Herkenhoff, A. Howard, B. Murray, in (3), pp. 767–798.
28. B. C. Murray *et. al.*, *Icarus* **17**, 328 (1972); L. A. Soderblom, M. C. Malin, J. A. Cutts, B. C. Murray, *J. Geophys. Res.* **78**, 4197 (1973); J. A. Cutts, *ibid.*, p. 4231.
29. K. R. Blasius, J. A. Cutts, A. D. Howard, *Icarus* **50**, 140 (1982).
30. K. E. Herkenhoff and B. C. Murray, *J. Geophys. Res.* **95**, 14511 (1990).
31. H. H. Kieffer, S. C. Chase, T. Z. Martin, E. D. Miner, F. D. Palluconi, *Science* **194**, 1341 (1976).
32. K. L. Tanaka and D. H. Scott, *U.S. Geol. Surv. Misc. Inv. Series Map I-1802-C* (1987).
33. J. J. Plaut, R. Kahn, E. A. Guinness, R. E. Arvidson, *Icarus* **75**, 357 (1988).
34. P. B. James, G. Briggs, J. Barnes, A. Spruck, *J. Geophys. Res.* **84**, 2889 (1979).
35. D. A. Paige and S. E. Wood, *Icarus* **99**, 15 (1992).
36. L_s is the angular position of Mars in its orbit as measured from the position of vernal equinox.
37. G. A. Briggs, W. A. Baum, J. Barnes, *J. Geophys. Res.* **84**, 2795 (1979).
38. P. B. James and K. Lumme, *Icarus* **50**, 368 (1982).
39. G. E. Hunt, A. O. Pickersgill, P. B. James, N. Evans, *Nature* **293**, 1 (1981).
40. R. Greeley, N. Lancaster, S. Lee, P. Thomas, in (3), pp. 730–766; R. A. Kahn, T. Z. Martin, R. W. Zurek, and S. W. Lee, in (3), pp. 1017–1053.
41. G. M. Keating *et al.*, *Science* **279**, 1672 (1998).

42. An experiment of the size and complexity of the MOC is truly a team effort; no one person, or even small group, can design, develop, fabricate, test, and operate such a device; we are deeply indebted to the literally hundreds of people without whom the Mars Observer, and later Mars Global Surveyor Camera, could not have been built and flown to Mars.

10 February 1998; accepted 17 February 1998